Structure and Calcium-Binding Studies of a Recoverin Mutant (E85Q) in an Allosteric Intermediate State†

James B. Ames,* Nobuko Hamasaki, and Tatiana Molchanova

Center for Advanced Research in Biotechnology, University of Maryland Biotechnology Institute, Rockville, Maryland 20850

Received December 13, 2001; Revised Manuscript Received March 14, 2002

ABSTRACT: Recoverin, a member of the EF-hand superfamily, serves as a calcium sensor in retinal rod cells. A myristoyl or related fatty acyl group covalently attached to the N-terminus of recoverin facilitates the binding of recoverin to retinal disk membranes by a mechanism known as the Ca^{2+}-myristoyl switch. Previous structural studies revealed that the myristoyl group of recoverin is sequestered inside the protein core in the absence of calcium. The cooperative binding of two calcium ions to the second and third EF-hands (EF-2 and EF-3) of recoverin leads to the extrusion of the fatty acid. Here we present nuclear magnetic resonance (NMR), fluorescence, and calcium-binding studies of a myristoylated recoverin mutant (myr-E85Q) designed to abolish high-affinity calcium binding to EF-2 and thereby trap the myristoylated protein with calcium bound solely to EF-3. Equilibrium calcium-binding studies confirm that only one Ca^{2+} binds to myr-E85Q under the conditions of this study with a dissociation constant of 100 μM. Fluorescence and NMR spectra of the Ca^{2+}-free myr-E85Q are identical to those of Ca^{2+}-free wild type, indicating that the E85Q mutation does not alter the stability and structure of the Ca^{2+}-free protein. In contrast, the fluorescence and NMR spectra of half-saturated myr-E85Q (one bound Ca^{2+}) look different from those of Ca^{2+}-saturated wild type (two bound Ca^{2+}), suggesting that half-saturated myr-E85Q may represent a structural intermediate. We report here the three-dimensional structure of Ca^{2+}-bound myr-E85Q as determined by NMR spectroscopy. The N-terminal myristoyl group of Ca^{2+}-bound myr-E85Q is sequestered within a hydrophobic cavity lined by many aromatic residues (F23, W31, Y53, F56, F83, and Y86) resembling that of Ca^{2+}-free recoverin. The structure of Ca^{2+}-bound myr-E85Q in the N-terminal region (residues 2−90) is similar to that of Ca^{2+}-free recoverin, whereas the C-terminal region (residues 100−202) is more similar to that of Ca^{2+}-bound wild type. Hence, the structure of Ca^{2+}-bound myr-E85Q represents a hybrid between the structures of recoverin with zero and two Ca^{2+} bound. The binding of Ca^{2+} to EF-3 leads to local structural changes within the EF-hand that alter the domain interface and cause a 45° swiveling of the N- and C-terminal domains, resulting in a partial unclamping of the myristoyl group. We propose that Ca^{2+}-bound myr-E85Q may represent a stable intermediate state in the kinetic mechanism of the calcium−myristoyl switch.

Calcium ion (Ca^{2+}) in retinal rod cells plays a critical role in regulating the phototransduction cascade in vision (*1*−*3*). Recoverin, a 23 kDa Ca^{2+}-binding protein and member of the EF-hand superfamily, serves as a Ca^{2+} sensor in retinal rods (*4*). Recoverin prolongs the lifetime of photoexcited rhodopsin by inhibiting rhodopsin kinase only at high Ca^{2+} levels (*5*−*7*). Hence, recoverin makes the desensitization of rhodopsin sensitive to Ca^{2+}, and the shortened lifetime of photoexcited rhodopsin at low Ca^{2+} levels may promote visual recovery and contribute to the adaptation to background light. Recoverin was also identified as the antigen in cancer-associated retinopathy, an autoimmune disease of the retina caused by a primary tumor in another tissue (*8*, *9*).

Recoverin contains four EF-hand Ca^{2+}-binding motifs and a myristoyl or related fatty acyl group covalently attached at the N-terminus (*10*). The cooperative binding of two Ca^{2+} to the second and third EF-hands (EF-2 and EF-3) induces the binding of myristoylated, but not unmyristoylated, recoverin to rod outer segment disk membranes (*11*, *12*). The three-dimensional structures of myristoylated recoverin with zero and two Ca^{2+} bound have been determined by NMR spectroscopy (*13*, *14*). A striking feature of these structures is the large Ca^{2+}-induced conformational change. In the Ca^{2+}-free state, the myristoyl group is sequestered in a deep hydrophobic cavity and is clamped by many aromatic residues. The binding of two Ca^{2+} leads to the extrusion of the myristoyl group that is accompanied by a 45° rotation of the two domains of the protein, and many hydrophobic residues (that contact the myristoyl group in the Ca^{2+}-free state) are exposed. The Ca^{2+}-induced exposure of the myristoyl group, termed the Ca^{2+}-myristoyl switch, enables recoverin to bind to membranes at high Ca^{2+}.

To gain insight into the kinetic mechanism of the Ca^{2+}−myristoyl switch, we wanted to examine the structure of intermediate species of recoverin containing only one Ca^{2+} bound. Previous studies including the current study have argued that the binding of two Ca^{2+} to recoverin is ordered

† This work was supported by NIH Grant EY12347 and a Beckman Young Investigator Award to J.B.A.

* Corresponding author. Phone: (301) 738-6120. Fax: (301) 738-6255. E-mail: james@carb.nist.gov.

10.1021/bi012153k CCC: $22.00 © 2002 American Chemical Society
Published on Web 04/16/2002

because Ca^{2+} binds to EF-3 with markedly higher intrinsic affinity than it does to EF-2 (*15*−*17*). Consistent with this view, Ca^{2+}-binding studies performed on the myristoylated recoverin mutant (E121Q) in which EF-3 is inactivated (*17*) revealed that the E121Q mutant protein does not exhibit any Ca^{2+}-induced conformational changes, suggesting that EF-2 does not bind Ca^{2+} when EF-3 is disabled. Hence, the ordered binding of calcium to EF-3 appears essential to facilitate the subsequent binding of Ca^{2+} to EF-2 in the myristoylated protein. Furthermore, the X-ray crystal structure of the unmyristoylated protein in the presence of half-saturating Ca^{2+} contains Ca^{2+} bound solely to EF-3 while EF-2 is unoccupied (*18*). The overall structure of unmyristoylated recoverin with one Ca^{2+} bound looks very similar to the structure of myristoylated recoverin containing two Ca^{2+} bound (*14*). The similarity of these structures might suggest that the binding of Ca^{2+} to EF-3 alone might be sufficient to drive the protein conformational changes involved in the Ca^{2+}−myristoyl switch (*19*). However, a Hill slope of two observed for Ca^{2+} binding to myristoylated recoverin in the presence of membranes (*11*) and/or rhodopsin kinase (*20*, *21*) indicates that the binding of *two* Ca^{2+} are required to drive the Ca^{2+}−myristoyl switch and inhibition of the kinase. The highly cooperative binding of Ca^{2+} to myristoylated recoverin prevents the accumulation of any intermediate species containing only one bound Ca^{2+} at equilibrium (*15*).

To assess structural changes in the myristoylated protein induced solely by the binding of Ca^{2+} to EF-3, we constructed a mutant that selectively and markedly impairs the binding of Ca^{2+} to EF-2. The substitution of E85 (in the Ca^{2+}-binding loop of EF-2) with the neutral residue glutamine (Q) eliminates an important negatively charged chelating group and has been shown previously to drastically decrease the affinity and binding of calcium to EF-2 (*17*, *19*, *22*). We report NMR, fluorescence, and equilibrium calcium-binding studies of myristoylated recoverin containing the mutation E85Q (myr-E85Q)[1] and thereby characterize the three-dimensional structure and Ca^{2+}-binding properties of myristoylated recoverin containing one Ca^{2+} bound to EF-3.

EXPERIMENTAL PROCEDURES

Site-Directed Mutagenesis. The single mutation E85Q was carried out by PCR-directed mutagenesis (*23*) using the QuikChange site-directed mutagenesis kit (Stratagene). The plasmid pTREC2 (*24*) was used as a template, and the following oligonucleotides were used as primers: 5′-CCA ACA GCG ATG GTA CCT TGG ACT TCA AGC AGT ATG TCA TCG-3′ and 5′-CGA TGA CAT ACT GCT TGA AGT CCA AGG TAC CAT CGC TGT TGG-3′. Introduction of the correct mutation was verified by sequencing the entire recoverin gene. The mutant gene was then subcloned into a vector pTISIDT at *Nde*I−*Xba*I sites.

Expression and Purification of Wild-Type and E85Q Myristoylated Recoverin. Both wild-type and myr-E85Q proteins were expressed in *Escherichia coli* strain DH5α cotransfected with plasmids pTREC2 and pBB131 as described previously (*11*). The cells were grown in LB broth at 32 °C until the cell culture reached an optical density of 0.7−0.8 at 600 nm. The myristoyl-CoA transferase expression was induced by adding IPTG (0.5 mM). Recoverin expression was induced 30 min later by rapidly raising the temperature to 42 °C and growing the cells for an additional 2 h. The protein purification procedure was similar to that used previously (*16*). Briefly, the cells were disrupted using a French pressure cell (Spectronic Instruments, Inc.), and the extract was clarified by centrifugation for 1.5 h at 4 °C. The crude extract was treated with $CaCl_2$ (3 mM), adsorbed onto a phenyl-Sepharose CL-4B (Pharmacia Biotech) column at 4 °C, and washed thoroughly using high Ca^{2+} buffer. The Ca^{2+}-free protein was eluted using Ca^{2+}-free buffer containing EGTA. The protein was further purified using Q-Sepharose chromatography at room temperature and then concentrated to a final concentration of 10 mg/mL using Centricon YM-10 (Millipore Corp.). The overall yields were 20 mg (wild type) and 10 mg (E85Q) from 1 L cultured cells. Proteins were aliquoted, frozen by liquid nitrogen, and stored at −80 °C. Protein concentrations in this study were determined by measuring the optical density at 280 nm and using a molar absorption coefficient $\epsilon = 23950\ cm^{-1}\ M^{-1}$ (*16*).

Binding of $^{45}Ca^{2+}$. Calcium-45 radioactive isotope (calcium-45, calcium chloride in aqueous solution, specfic activity = 850 mCi/mL, Amersham Pharmacia Biotech) was used to quantitate the binding of Ca^{2+} to recoverin. $^{45}Ca^{2+}$ binding to wild-type and E85Q recoverin was measured as the protein-bound radioactivity retained after ultrafiltration using a procedure (*25*) based on the original method of Paulus (*26*). Briefly, the buffer used in all Ca^{2+} titrations (50 mM HEPES, 0.1 M KCl, 1 mM DTT, pH 7.5) was decalcified using Analytical Grade Chelex resin (Bio-Rad Laboratories) using the batch method. Protein was decalcified by passing it through a PD-10 column (Sephadex G-25 M, 1.52 × 5 cm, bed volume 9.1 mL; Amersham Pharmacia Biotech) previously equilibrated in decalcified buffer. All tubing, glassware, and containers that contacted the sample were previously rinsed with 0.1 M HCl and then rinsed with decalcified buffer to remove any contaminating Ca^{2+}. A Centricon YM-10 concentrator (10 kDa cutoff, 2 mL sample compartment, Millipore Corp.) used in the titration was pretreated to remove contaminating Ca^{2+}. The lower chamber was rinsed with 0.1 M HCl followed by several rinses with decalcified buffer. The membrane was decalcified by rinsing with 5% $NaHCO_3$ followed by several rinses with decalcified buffer. Decalcified protein (1−1.5 mL, 70−150 μM) was placed into the sample compartment, and 12.4 μL of 0.25 mM $^{45}Ca^{2+}$ solution (2.6 μCi) was added. The sample was carefully mixed and centrifuged (2300 rpm, 2 min) using a tabletop centrifuge (Beckman Model TJ-6), forming 25 μL of filtrate. The filtrate was returned to the sample chamber, mixed, and centrifuged a second time. The radioactivity of the filtrate (free Ca^{2+}) and an equal volume of the protein sample (total Ca^{2+}) was determined by liquid scintillation counting (Liquid Scintillation Analyzer, Packard Instrument Co.). Additions of nonradioactive Ca^{2+} were made to the protein sample to adjust the total Ca^{2+} concentration throughout the titration, and the above centrifugation pro-

[1] Abbreviations: EDTA, *N*,*N*,*N*′,*N*′-ethylenediaminetetraacetic acid; EGTA, ethylene glycol bis(β-aminoethyl ether)-*N*,*N*,*N*′,*N*′-tetraacetic acid; HEPES, *N*-(2-hydroxyethyl)piperazine-*N*′-2-ethanesulfonic acid; HSQC, heteronuclear single-quantum coherence; IPTG, isopropyl thiogalactoside; myr-E85Q, myristoylated recoverin E85Q mutant; NOESY, nuclear Overhauser effect spectroscopy; RMS, root mean square; SDS−PAGE, sodium dodecyl sulfate−polyacrylamide gel electrophoresis.

cedure was repeated for each addition point in the titration. The free and bound Ca^{2+} concentrations were calculated from the measured radioactivity as described previously (*27*).

Fluorescence Spectroscopy. The intrinsic tryptophan fluorescence emission spectra of Ca^{2+}-free wild-type and E85Q myristoylated recoverin were obtained using 2 mL protein samples (2 μM protein concentration) dissolved in 20 mM Tris-HCl, 1 mM EGTA, and 0.1 M KCl, pH 8.0 at 25 °C. The Ca^{2+}-bound proteins were generated by the addition of $CaCl_2$ (2 mM). The fluorescence was excited at 290 nm to minimize any contribution from tyrosine. The fluorescence emission spectra were recorded at 305−440 nm with a 2-nm band-pass using a FluoroMax-2 fluorometer (Jobin YVON-SPEX, Instruments S.A., Inc.).

NMR Spectroscopy. Samples for NMR analysis were prepared by dissolving ^{15}N-labeled or $^{13}C/^{15}N$-labeled myr-E85Q (0.8 mM) in 0.5 mL of a 95% H_2O/5% $[^2H]H_2O$ solution containing 10 mM $[^2H_2]$imidazole (pH 6.8), 10 mM $[^2H_{10}]$dithiothreitol, 1 mM $MgCl_2$, and either 1 mM EDTA (Ca^{2+} free) or 1 mM $CaCl_2$ (Ca^{2+} bound). All NMR experiments were performed at 37 °C on a Bruker DRX-500 or DRX-600 spectrometer equipped with a four-channel interface and a triple-resonance probe with triple-axis pulsed field gradients. The $^{15}N-^1H$ HSQC spectra (see Figure 3) were recorded on a sample of ^{15}N-labeled myr-E85Q (in 95% H_2O, 5% ^2H_2O). The number of complex points and acquisition times were 256, 180 ms [^{15}N (F_1)] and 512, 64 ms [^1H (F_2)]. The $^{13}C-^1H$ HSQC spectra (see Figure 4) were recorded on a sample of unlabeled myr-E85Q protein containing a uniformly ^{13}C-labeled myristoyl group (*28*). All triple-resonance experiments were performed as described previously (*29*) on a sample of $^{13}C/^{15}N$-labeled myr-E85Q (in 95% H_2O, 5% ^2H_2O) with the following number of complex points and acquisition times: HNCO [^{15}N (F_1) 32, 23.7 ms; ^{13}CO (F_2) 64, 42.7 ms; ^1H (F_3) 512, 64 ms], HNCACB [^{15}N (F_1) 32, 23.7 ms; ^{13}C (F_2) 48, 6.3 ms; ^1H (F_3) 512, 64 ms], CBCACONNH [^{15}N (F_1) 32, 23.7 ms; ^{13}C (F_2) 48, 6.3 ms; ^1H (F_3) 512, 64 ms], CBCACOCAHA [^{13}C (F_1) 52, 6.8 ms; ^{13}CO (F_2) 64, 42 ms; ^1H (F_3) 384, 64 ms], and HBHACONNH [^{15}N (F_1) 32, 23.7 ms; $^1H_{ab}$ (F_2) 64, 21 ms; ^1H (F_3) 512, 64 ms]. The triple-resonance spectra were processed and analyzed as described previously (*29*).

NMR Structure Calculations. Backbone and side-chain NMR resonances of myr-E85Q were assigned as described previously (*29*). Structure calculations for myr-E85Q were performed using the YASAP protocol within X-PLOR (*30*, *31*), as described previously (*32*). A total of 2050 interproton distance constraints was obtained as described (*29*) by analysis of ^{13}C-edited and ^{15}N-edited NOESY-HSQC spectra (120 ms mixing time) of $^{13}C,^{15}N$-labeled Frq1. In addition to the NOE-derived distance constraints, the following additional constraints were included in the structure calculation: 6 distance constraints involving Ca^{2+} bound to loop residues 1, 3, 5, 7, and 12 in EF-3; 150 distance constraints for 75 hydrogen bonds; and 230 dihedral angle constraints. Forty independent structures were calculated, and the 15 structures of lowest energy were selected. The average total and experimental distance energies are 4053 and 104 kcal mol^{-1} (calculated with the use of square-well potentials with a force constant of 50 kcal mol^{-1} $Å^2$). The average root-mean-square (RMS) deviations from an idealized geometry for bonds and angles are 0.0074 Å and 2.07°. None of the distance and angle constraints were violated by more than 0.40 Å or 4°, respectively.

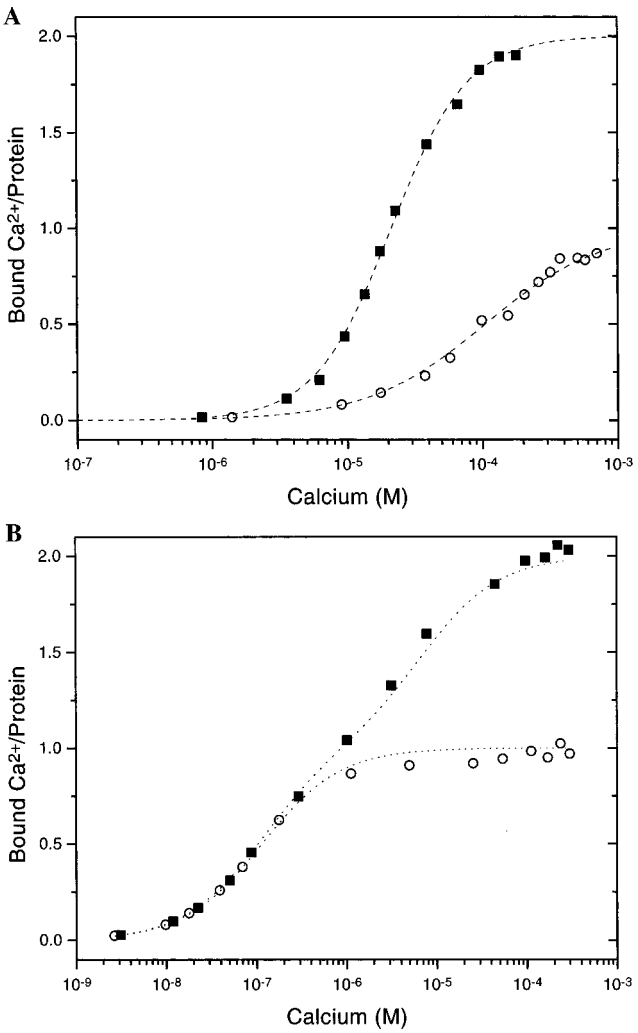

FIGURE 1: Equilibrium Ca^{2+} binding to myristoylated (A) and unmyristoylated (B) recoverin. Titrations of $^{45}Ca^{2+}$ to wild type (filled squares) and to the E85Q mutant (open circles) were conducted using an ultrafiltration method, as described in Experimental Procedures. The number of ions bound per molecule of protein is plotted versus the free calcium concentration. Dotted lines represent the best fit to the Hill model (K_d = 0.15, 20, and 100 μM for unmyristoylated E85Q, myristoylated wild type, and myr-E85Q, respectively) and to a two-site model (K_{d1} = 0.1 μM and K_{d2} = 7 μM for unmyristoylated wild-type recoverin).

RESULTS

Equilibrium Ca^{2+}-Binding Measurements. Recoverin contains four EF-hand Ca^{2+}-binding motifs (EF-1, residues 27−56; EF-2, residues 63−92; EF-3, residues 101−130; and EF-4, residues 149−178). The amino acid sequence of the loop regions of EF-1 and EF-4 contain substitutions (EF-1, K37, C39, and P40; and EF-4, G160 and K162) that disrupt their respective binding loops and prevent Ca^{2+} binding, as seen in the crystal structures of recoverin (*18*), frequenin (*33*), and neurocalcin (*34*). By contrast, the sequences of EF-2 and EF-3 are good matches to the consensus and have been shown previously to bind Ca^{2+} (*15*, *22*).

Equilibrium measurements of $^{45}Ca^{2+}$ binding were conducted on wild-type and E85Q myristoylated recoverin (Figure 1A). At saturation, two Ca^{2+} bind to the wild-type

protein, whereas only one Ca^{2+} binds to myr-E85Q. The fractional saturation (Y), which can be obtained from the same data, can be represented by the Hill equation:

$$Y = \frac{[Ca^{2+}]^a}{[Ca^{2+}]^a + K_d{}^a} \quad (1)$$

where $[Ca^{2+}]$ is the free Ca^{2+} concentration, K_d is the apparent dissociation constant, and a denotes the Hill coefficient. On the basis of our analysis of the data in Figure 1, we determined that wild-type myristoylated recoverin binds two Ca^{2+} with a K_d of 20 μM and Hill coefficient of 1.5, similar to that observed previously (*15*, *16*). Our analysis also revealed that myr-E85Q binds only one Ca^{2+} with a K_d of 100 μM and Hill coefficient of 1. The substantially higher apparent K_d observed for the myr-E85Q protein compared to wild type suggests that much of the binding energy of Ca^{2+} bound to EF-3 may be used to drive a large protein conformational change. The binding stoichiometry and Hill slope of 1 observed for the myr-E85Q protein strongly argues that only one Ca^{2+} is bound to the protein at EF-3, and the E85Q mutation does indeed abolish binding of Ca^{2+} to EF-2 under the conditions of this study.

Unmyristoylated wild-type recoverin exhibits biphasic binding of Ca^{2+} (Figure 1B), indicating two sites with markedly different intrinsic affinities. The microscopic dissociation constants measured for the two sites ($K_{d1} = 0.12$ μM and $K_{d2} = 7$ μM) are similar to those observed previously (*15*, *16*). The unmyristoylated E85Q mutant binds one Ca^{2+} at saturation with a K_d equal to 0.15 μM but lacks any lower affinity binding at Ca^{2+} levels out to 1 mM (Figure 1B). These binding data demonstrate that EF-3 represents the higher affinity site and that EF-2 is unoccupied in the E85Q mutant under these conditions. Hence, wild-type recoverin binds two Ca^{2+} in an ordered fashion where EF-3 binds Ca^{2+} first due to its higher intrinsic affinity, followed by subsequent and lower affinity binding of Ca^{2+} to EF-2. The ordered binding determined for unmyristoylated recoverin should also be valid for the myristoylated protein because the myristoyl group does not affect the *microscopic* Ca^{2+} affinities of EF-2 and EF-3 (*15*). It is important to point out, however, that the lower *apparent* Ca^{2+} affinity of the myristoylated protein (Figure 1A) compared to that of unmyristoylated recoverin (Figure 1B) is most likely due to an allosteric conformational transition induced by the attached myristoyl group as described previously (*15*, *16*). The myristoyl group lowers the apparent affinity of the protein for Ca^{2+} by preferentially stabilizing the Ca^{2+}-free "T" form of the protein (sequestered fatty acid) over the Ca^{2+}-bound "R" form (extruded myristate). In essence, the myristoyl group serves as a built-in allosteric effector because the extrusion of the myristoyl group during T → R is energetically unfavorable. Therefore, much of the Ca^{2+}-binding energy is harnessed to drive the unfavorable extrusion of the myristoyl group. In contrast, the Ca^{2+}-binding energy of the unmyristoylated protein is not coupled to an unfavorable extrusion, resulting in the much higher apparent affinity for Ca^{2+}.

Fluorescence Spectroscopy To Monitor Ca^{2+}-Induced Conformational Changes. As one means to evaluate whether myr-E85Q adopts an intermediate protein structure upon Ca^{2+} binding, we compared the effect of Ca^{2+} on the intrinsic tryptophan fluorescence of wild type and myr-E85Q, both of which contain three tryptophan residues (W31, W104, and W156). The fluorescence emission of tryptophan is sensitive to its surrounding chemical environment and, hence, provides an effective probe of structural changes in a protein (*35*). In the absence of Ca^{2+}, the fluorescence emission spectra of wild type and myr-E85Q were nearly identical (Figure 2), suggesting that the E85Q mutation does not alter significantly the overall structure of the Ca^{2+}-free protein. Correspondingly, the folding stability of Ca^{2+}-free myr-E85Q was also shown to be similar to that of wild type (*17*). Upon Ca^{2+} binding to either wild type or myr-E85Q, the emission maximum shifted to longer wavelength (10 nm for wild type and 6 nm for myr-E85Q) and, at saturation, the emission intensity increased by 20% for wild type and decreased by 15% for myr-E85Q (Figure 2), similar to spectra observed previously (*19*). These spectral differences suggest that the structure of half-saturated myr-E85Q may be significantly different from those of Ca^{2+}-free and Ca^{2+}-bound forms of wild type and may represent the structure of an intermediate state. On the basis of first principles (*35*), the Ca^{2+}-induced spectral change observed for myr-E85Q suggests that one or more tryptophan residues shift into a more polar chemical environment when the protein is in its Ca^{2+}-bound state relative to its Ca^{2+}-free state. On the basis of our structures of recoverin (see below), the binding of Ca^{2+} to EF-3 leads to structural changes that cause W104 in the E-helix of EF-3 to become more solvent exposed whereas the chemical environments of W31 and W156 do not change appreciably in the intermediate state. The binding of a second Ca^{2+} to recoverin at EF-2 results in structural changes in the N-terminal domain that alter the chemical environment of W31, resulting in a large increase in its fluorescence intensity (larger than the decrease for W104). The overall effect is a net increase in fluorescence intensity with a red shift in the spectrum for Ca^{2+}-bound wild type compared to that of Ca^{2+}-free wild type.

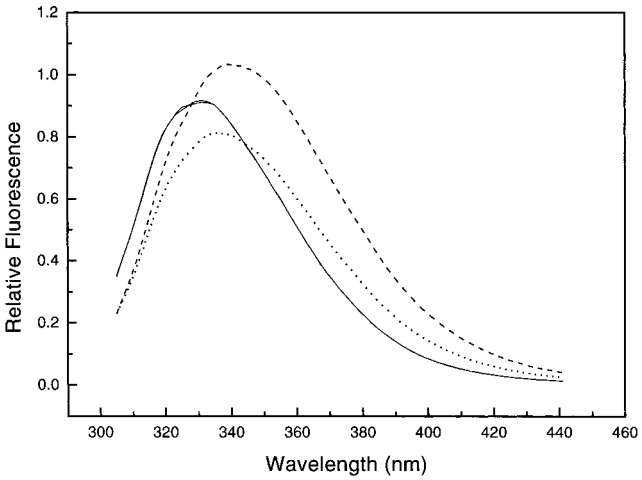

FIGURE 2: Effect of Ca^{2+} on intrinsic tryptophan fluorescence spectra of myristoylated recoverin. Fluorescence emission spectra for Ca^{2+}-free forms of wild type and myr-E85Q (solid lines), Ca^{2+}-bound wild type (dashed line), and Ca^{2+}-bound myr-E85Q (dotted line). Fluorescence was excited by 290 nm light to minimize any contribution from tyrosine.

Structural Studies Using NMR. Conformational changes in myr-E85Q resulting from Ca^{2+} binding were also moni-

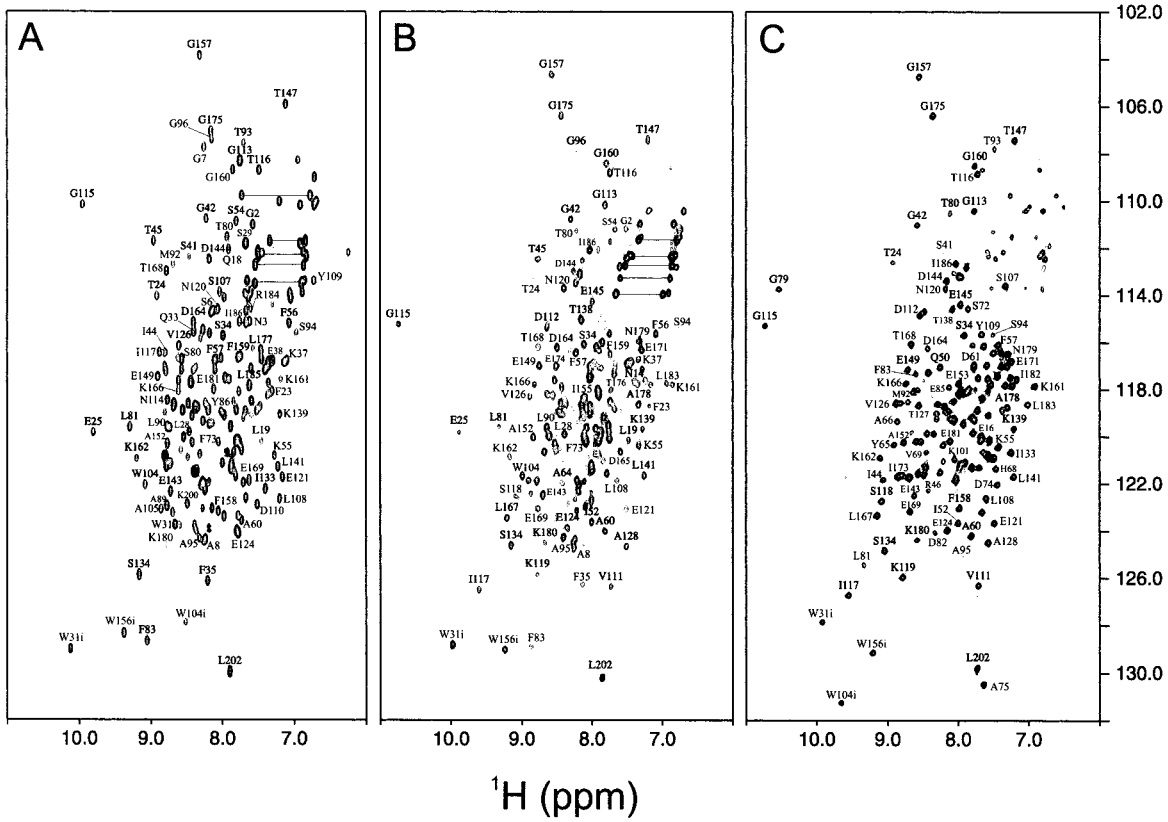

FIGURE 3: Two-dimensional ^{15}N−^{1}H HSQC NMR spectra of myristoylated recoverin. Two-dimensional ^{15}N−^{1}H HSQC NMR spectra for Ca^{2+}-free myr-E85Q (A), Ca^{2+}-bound myr-E85Q (B), and Ca^{2+}-bound wild type (C), each uniformly labeled with nitrogen-15, were recorded at 600 MHz ^{1}H frequency. Peaks corresponding to the $-NH_2$ groups of the side-chain amides of Q and N residues are connected by dotted lines. Sequence-specific assignments are indicated, and the assignments for Ca^{2+}-bound myr-E85Q have been deposited into BioMagRes NMR Databank (accession no. 5332).

tored by nuclear magnetic resonance (NMR) spectroscopy. Two-dimensional NMR spectra (^{1}H−^{15}N HSQC) of uniformly ^{15}N-labeled Ca^{2+}-free and Ca^{2+}-bound forms of myr-E85Q and wild type were collected (Figure 3). Peaks in each spectrum represent main-chain and side-chain amide protons that serve as fingerprints of overall conformation. The NMR spectrum of Ca^{2+}-free myr-E85Q (Figure 3A) is nearly identical to that of Ca^{2+}-free wild type (*36*). The similarity of these spectra demonstrates that the E85Q mutation does not alter the structure of the Ca^{2+}-free protein. In contrast, the NMR spectrum of myr-E85Q obtained at 1 molar equiv of Ca^{2+} (Figure 3B) is different from the spectra of the Ca^{2+}-free (Figure 3A) and Ca^{2+}-saturated (Figure 3C) wild-type protein. These spectral differences suggest that half-saturated myr-E85Q may represent a structural intermediate. The chemical shift frequencies of the NMR peaks of half-saturated myr-E85Q (Figure 3B) assigned to residues in the N-terminal region (residues 2−90) correspond closely to the chemical shifts assigned to N-terminal residues of the Ca^{2+}-free protein (Figure 3A). In contrast, the NMR frequencies assigned to C-terminal residues of half-saturated myr-E85Q (residues 101−202) are more similar to those of Ca^{2+}-saturated wild type (Figure 3C). The NMR spectrum (and therefore structure) of half-saturated myr-E85Q (Figure 3B) represents a hybrid of the spectra (and structures) of the wild-type protein containing zero and two Ca^{2+} bound (Figure 3A,C). To check whether myr-E85Q could be driven into a wild-type-like fully saturated state, NMR spectra of myr-E85Q were recorded at much higher Ca^{2+} concentrations, ranging from 10 to 100 mM (data not shown). The very high Ca^{2+} levels (>10 mM) caused spectral shifts for resonances assigned to residues in EF-2, suggesting that a second Ca^{2+} might bind very weakly to the myr-E85Q protein. However, the overall spectrum of myrE85Q at very high Ca^{2+} is more similar to that of half-saturated myr-E85Q (Figure 3B) than that of Ca^{2+}-saturated wild type (Figure 3C), suggesting that, at the high Ca^{2+} levels, the myr-E85Q protein may not be completely driven into a wild-type-like fully saturated state.

NMR Analysis of [^{13}C]Myristate-Labeled E85Q. A series of NMR experiments (two-dimensional ^{1}H−^{13}C HSQC and three-dimensional ^{13}C-filtered NOESY-HMQC) were performed on samples of myr-E85Q that contained a ^{13}C-labeled myristoyl group and were analyzed to probe the chemical environment around the fatty acyl chain (*28*, *29*). The peaks in the ^{1}H−^{13}C HSQC spectra in Figure 4 represent protons that are covalently linked to ^{13}C so that only the methylene and methyl proton resonances of the labeled fatty acyl chain appear in these spectra. The spectrum of the myristoyl group in Ca^{2+}-free myr-E85Q is identical to that of Ca^{2+}-free wild type and exhibits doublet peaks in the ^{1}H dimension assigned to methylene protons at positions 2, 3, 11, and 12 (Figure 4A). The protein environment of the highly sequestered myristoyl group causes the pairs of methylene protons attached to the fatty acyl chain to become magnetically inequivalent, giving rise to doublet peaks that represent each methylene proton pair. The addition of saturating Ca^{2+} to myr-E85Q leads to striking spectral changes in the ^{1}H−^{13}C HSQC spectrum of the labeled myristoyl group (Figure 4B), indicating a Ca^{2+}-induced environmental change of the fatty acid. All of the myristoyl group resonances become single

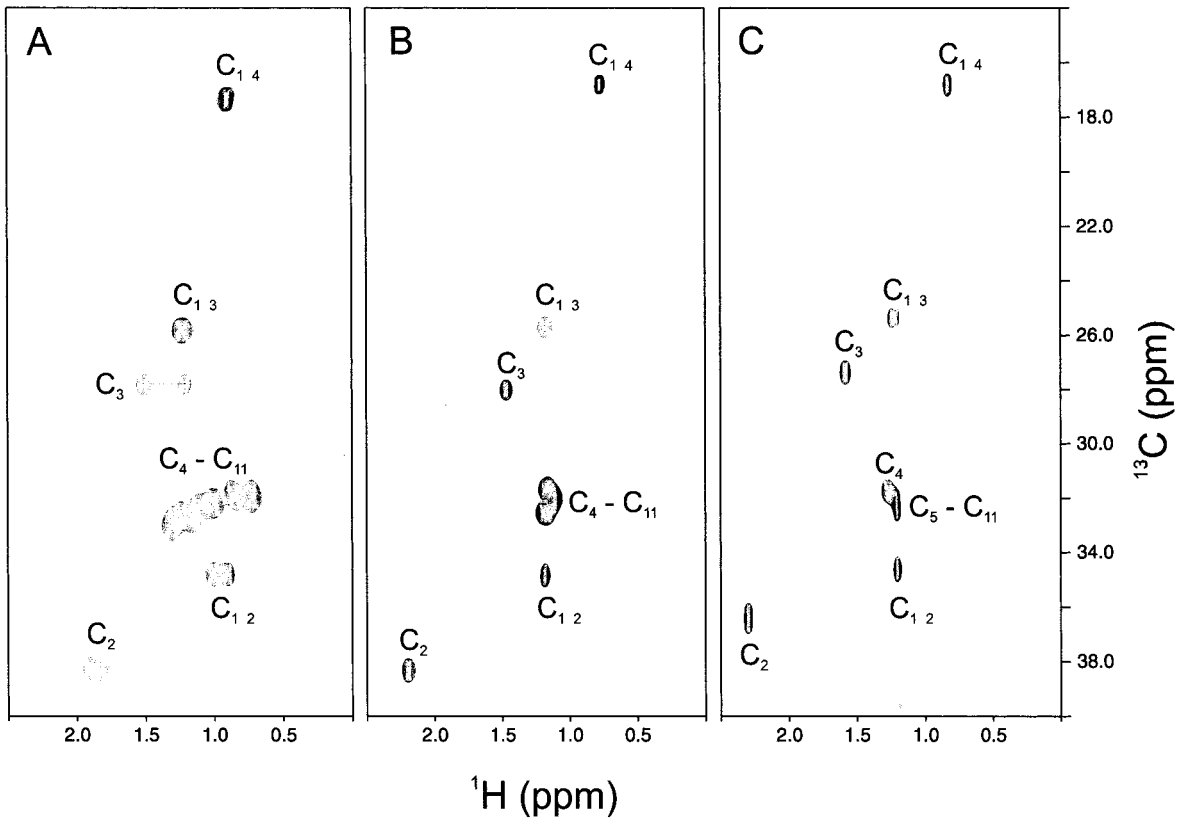

FIGURE 4: The myristoyl group of Ca^{2+}-bound myr-E85Q is partially solvent exposed. Two-dimensional ($^1H-^{13}C$ HSQC) NMR spectra of the myristoyl group of Ca^{2+}-free (A) and Ca^{2+}-bound (B) myr-E85Q and free myristic acid dissolved in chloroform (C). The myristoyl group was labeled with carbon-13, and the protein was unlabeled. The peaks in the spectrum represent protons attached to ^{13}C-labeled fatty acyl chain.

peaks, suggesting that the fatty acid may be located in a more dynamic and/or isotropic chemical environment in the Ca^{2+}-bound protein. The chemical shifts of the methylene protons at positions 2, 3, and 4 of Ca^{2+}-bound myr-E85Q (Figure 3B) are similar to those of myristic acid free in solution (Figure 4C), suggesting that part of the fatty acyl chain of Ca^{2+}-bound myr-E85Q may be solvent exposed.

To further test whether the myristoyl group of Ca^{2+}-bound myr-E85Q is solvent-exposed, three-dimensional ($^{13}C/F_1$)-edited and ($^{13}C/F_3$)-filtered NOESY experiments were performed on unlabeled E85Q protein containing a ^{13}C-labeled myristate. These spectra selectively probed atoms of residues in the protein that lie within 5 Å of the ^{13}C-labeled fatty acyl chain. Nuclear Overhauser effect (NOE) dipolar interactions between the myristate C_{14}-methyl group ($^{13}C_{14}$: $F_2 =$ 16.9 ppm) and the protein are displayed in the NOESY spectrum in Figure 5. The spectra of Ca^{2+}-free (Figure 5A) and Ca^{2+}-bound (Figure 5B) myr-E85Q both exhibit many off-diagonal peaks assigned to aromatic ring protons (Y53, F56, F83, and Y86) and aliphatic protons (I52 and L14). Therefore, the methyl group of myristate interacts intimately with the protein and is buried in a similar hydrophobic cavity in both the Ca^{2+}-free and Ca^{2+}-bound forms of myr-E85Q. In the Ca^{2+}-free protein, the myristate methylene protons near the carbonyl end (at positions 2 and 3) exhibit NOE dipolar interactions with side-chain resonances from W104 and L108. In contrast, no such dipolar interactions with myristate protons at positions 2 and 3 were observed for the Ca^{2+}-bound E85Q protein (data not shown), suggesting that the carbonyl end of the myristoyl group may be solvent exposed in Ca^{2+}-bound myr-E85Q.

Three-Dimensional Structure of Ca^{2+}-Bound Myr-E85Q. The number of peaks observed in the $^1H-^{15}N$ HSQC NMR spectrum of Ca^{2+}-bound myr-E85Q (Figure 3B) closely matched the expected number amide protons throughout the protein, indicating that it should be feasible to determine its full three-dimensional structure by NMR. However, some resonances from residues in the N-terminal domain (residues 74−78) exhibited very weak NMR intensities and were not analyzed in this study. To elucidate the structure, resonances in the NMR spectrum were assigned to specific amino acid residues. Triple-resonance experiments correlating ^{15}N, ^{13}C, and ^1H were performed and analyzed in making the assignments (see Experimental Procedures). Over 90% of the backbone resonances were assigned as indicated in Figure 3B, and the assignments have been deposited into the BioMagResBank (accession no. 5332). These backbone assignments then served the basis for assigning about 75% of side-chain resonances. To calculate the three-dimensional structure, more than 2000 proton−proton distance relationships (derived from nuclear Overhauser effect data) and more than 230 dihedral angle restraints (derived from *J*-coupling and chemical shift data) were applied using distance geometry and restrained molecular dynamics (see Experimental Procedures).

The ensemble of lowest energy structures of Ca^{2+}-bound E85Q calculated on the basis of the NMR data are shown in Figure 6A, and the average main-chain structure is depicted as a ribbon diagram (Figure 6B). The NMR-derived structures of Ca^{2+}-bound E85Q have been deposited into the Protein Data Bank (1LA3). The structure of the entire polypeptide main chain has been defined except for disor-

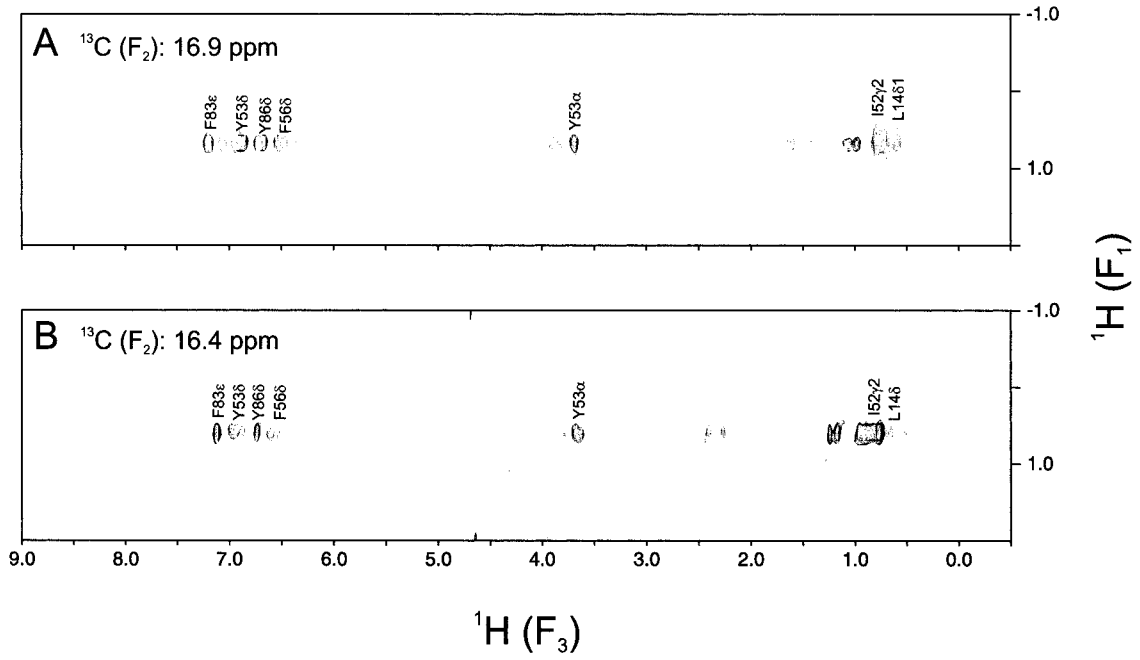

FIGURE 5: The myristoyl methyl group is sequestered inside myr-E85Q protein. Three-dimensional ($^{13}C/F_1$)-edited, ($^{13}C/F_3$)-filtered HMQC-NOESY spectra of Ca^{2+}-free (A) and Ca^{2+}-bound (B) myr-E85Q. The myristoyl group was labeled with ^{13}C (99%), and the protein was unlabeled. Selected slices at $F_2 = 16.9$ and 16.4 ppm are shown to selectively probe interactions between the myristoyl methyl group and residues of the protein that are spatially close to the methyl end of myristate.

dered regions in the loops of EF-2 (residues 74−78) and EF-4 (residues 160−164) and at the carboxyl terminus (residues 190−202). The secondary structure of Ca^{2+}-bound E85Q is very similar to that seen in previous structures of recoverin (*13*, *14*, *18*). However, the overall tertiary fold of Ca^{2+}-bound E85Q is very different from the overall folds of recoverin with zero and two Ca^{2+} bound (Figure 7). The overall RMS deviations of all main-chain atoms are 9.3 and 7.0 Å in comparing Ca^{2+}-bound myr-E85Q with Ca^{2+}-free and Ca^{2+}-bound wild type, respectively. Ca^{2+}-bound myr-E85Q, like Ca^{2+}-free and Ca^{2+}-bound wild type, contains two tightly packed and interacting domains. Each domain contains a pair of EF-hand motifs: EF-1 and EF-2 are in the N-terminal domain, and EF-3 and EF-4 occupy the C-terminal domain.

The structure of the N-terminal domain (residues 2−92, shown green and red in Figures 6 and 7) of Ca^{2+}-bound myr-E85Q partially resembles that of Ca^{2+}-free wild type (Figure 7A) and is very different from that of Ca^{2+}-bound wild type (Figure 7C). The RMS deviations of the main-chain atoms in the N-terminal domain are 1.6 and 7.7 Å in comparing Ca^{2+}-bound myr-E85Q with Ca^{2+}-free and Ca^{2+}-bound wild type, respectively. Most striking in the N-terminal domain of Ca^{2+}-bound myr-E85Q is that the myristoyl group is flanked by a long N-terminal helix (residues 5−17, shaded pink in Figure 6B) and is sequestered in a hydrophobic cavity containing many aromatic residues from EF-1 and EF-2 (W31, Y32, F49, Y53, F56, F83, and Y86; Figure 8). An important difference between Ca^{2+}-free wild type (Figure 8A) and Ca^{2+}-bound myr-E85Q (Figure 8B) is that the carbonyl end of the fatty acyl group in Ca^{2+}-bound E85Q is somewhat more solvent exposed and does not interact with any hydrophobic residues from EF-3 (W104 and L108).

The structure of the C-terminal domain (residues 101−202, cyan and yellow in Figures 6 and 7) of Ca^{2+}-bound myr-E85Q (Figures 6B and 7B) is similar to that of Ca^{2+}-bound wild type (Figure 7C). The RMS deviation of the main-chain atoms in the C-terminal domain is 1.25 Å in comparing Ca^{2+}-bound myr-E85Q with Ca^{2+}-bound wild type. In Ca^{2+}-bound myr-E85Q, the entering helix of EF-2 (residues 63−73) packs against the helices of EF-3 (residues 101−109 and 119−130) at the interface between the two domains, similar to that of Ca^{2+}-bound wild type (see residues H68 and L108 in Figure 7B,C). The linker between the two domains is U-shaped, which positions the four EF-hands in a tandem array like that of Ca^{2+}-bound wild type and unlike the dumbbell arrangement found in calmodulin (*37*) and troponin C (*38*). The structure of EF-3 in Ca^{2+}-bound myr-E85Q is similar to that of Ca^{2+}-bound wild type. The RMS deviations of the main-chain atoms of EF-3 are 0.6 Å in comparing Ca^{2+}-bound myr-E85Q with wild type and 0.85 Å in comparing Ca^{2+}-bound myr-E85Q with calmodulin. Likewise, the coordination of Ca^{2+} is virtually identical in all three.

The structures of EF-1 (residues 27−56) and EF-2 (residues 63−92) in Ca^{2+}-bound E85Q are somewhat similar to those of Ca^{2+}-free wild type and are very different from those of Ca^{2+}-bound wild type. Conversely, the structures of EF-3 (residues 101−130) and EF-4 (residues 148−177) in Ca^{2+}-bound myr-E85Q are more similar to those of Ca^{2+}-bound wild type. The RMS deviations of the main-chain atoms of the EF-hands are 0.53 Å (EF-1), 1.5 Å (EF-2), 2.5 Å (EF-3), and 2.2 Å (EF-4) in comparing Ca^{2+}-bound myr-E85Q with Ca^{2+}-free wild type. Conversely, the RMS deviations of the main-chain atoms of the EF-hands are 3.9 Å (EF-1), 3.1 Å (EF-2), 0.6 Å (EF-3), and 1.4 Å (EF-4) in comparing Ca^{2+}-bound myr-E85Q with Ca^{2+}-bound wild type. The interhelical angles of the EF-hands as defined by Zhang et al. (*39*) follow a similar trend (Table 1). The interhelical angles of EF-1 and EF-2 of Ca^{2+}-bound myr-E85Q are similar to those of Ca^{2+}-free wild type and differ from those of Ca^{2+}-bound wild type. Conversely, the

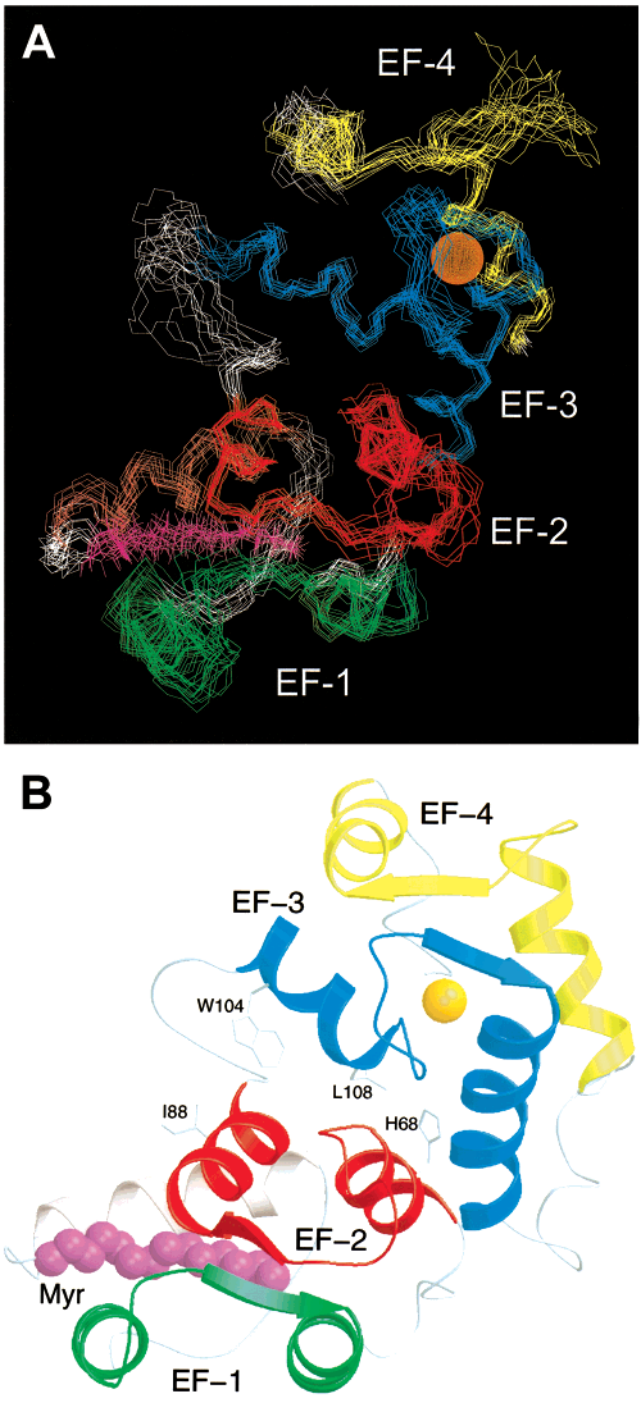

FIGURE 6: Three-dimensional structure of Ca^{2+}-bound myr-E85Q by NMR. Superposition of main-chain atoms of 20 NMR-derived structures (A) and schematic ribbon diagram of the energy-minimized average structure (B) of myr-E85Q with one Ca^{2+} bound. The root-mean-square deviation of the NMR-derived structures relative to the mean structure is 0.8 Å for main-chain atoms and 1.4 Å for all non-hydrogen atoms in the regions of regular secondary structure. Atomic coordinates have been deposited in the Protein Data Bank (entry 1LA3).

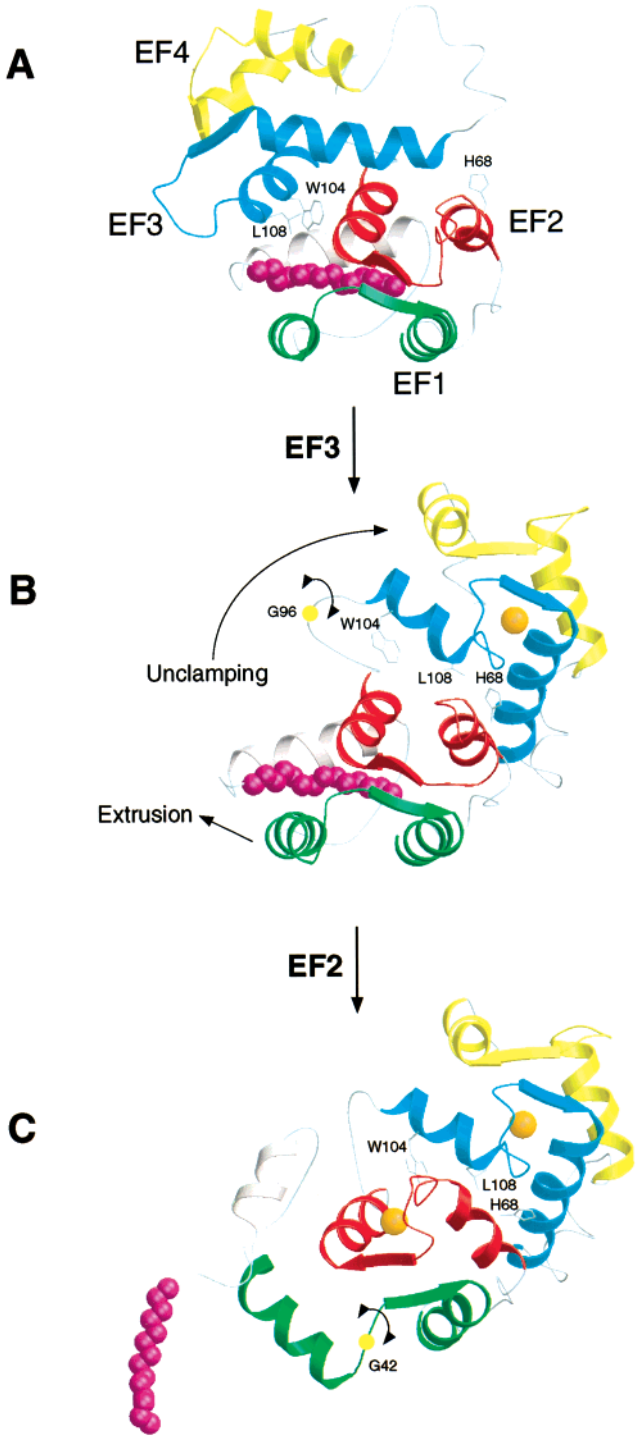

FIGURE 7: Sequential kinetic mechanism of the Ca^{2+}-myristoyl switch. Three-dimensional structures of myristoylated recoverin with zero Ca^{2+} bound (*13*) (A), one Ca^{2+} bound (determined in this study) (B), and two Ca^{2+} bound (*14*) (C). The first step of the mechanism involves the binding of Ca^{2+} to EF-3 that causes minor structural changes within the EF-hand that sterically promote a 45° swiveling of the two domains, resulting in a partial unclamping of the myristoyl group and a dramatic rearrangement at the domain interface. The resulting altered interaction between EF-2 and EF-3 potentiates the binding of a second Ca^{2+} to the protein at EF-2 in the second step, which causes structural changes within the N-terminal domain that directly lead to the ejection of the fatty acyl group.

interhelical angles of EF-3 and EF-4 of Ca^{2+}-bound myr-E85Q are more similar to those of Ca^{2+}-bound wild type.

A detailed comparison of the structures of Ca^{2+}-free and Ca^{2+}-bound EF-3 reveals how a small and localized Ca^{2+}-induced structural change within EF-3 leads to a large relative displacement of EF-2 at the domain interface (Figure 9). The overall Ca^{2+}-induced structural change within EF-3 is relatively small. The RMS deviation is only 2.5 Å in comparing the main-chain atoms of Ca^{2+}-free and Ca^{2+}-bound EF-3 (see Ca^{2+}-free and Ca^{2+}-bound EF-3 represented

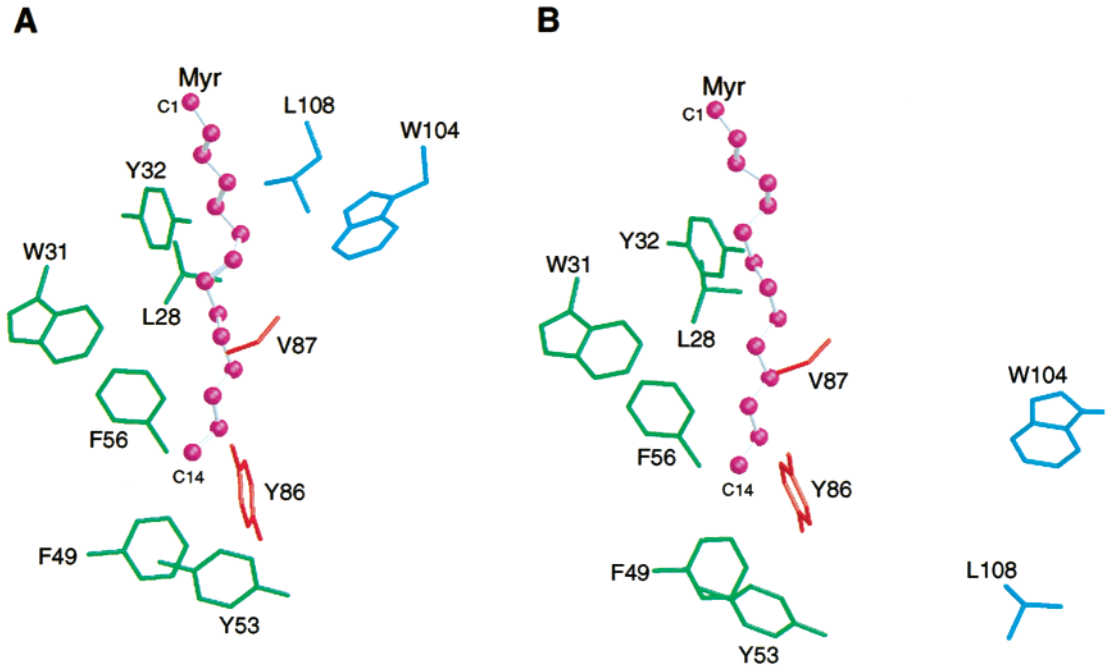

FIGURE 8: Structural environment of the myristoyl group. Side-chain atoms of protein residues located less than 5 Å from the fatty acyl chain of Ca^{2+}-free wild type (A) and Ca^{2+}-bound myr-E85Q (B) are depicted in a ball-and-stick representation. Atoms from the fatty acyl chain are highlighted in magenta. Side-chain atoms from residues of EF-1, EF-2, and EF-3 are colored green, red, and cyan, respectively.

Table 1: Interhelical Angles (in deg) of the EF-Hands of Myristoylated Recoverin As Defined by Ref *39* [a]

structure	EF-1	EF-2	EF-3	EF-4
Ca^{2+}-bound wild type	114 ± 8	121 ± 6	92 ± 5	90 ± 5
Ca^{2+}-free wild type	172 ± 7	135 ± 5	118 ± 5	102 ± 4
Ca^{2+}-bound myr-E85Q	169 ± 12	128 ± 5	91 ± 5	92 ± 5

[a] The angles were derived from the ensemble on NMR structures of Ca^{2+}-free wild type (*13*), Ca^{2+}-bound myr-E85Q (this study), and Ca^{2+}-bound wild type (*14*). The uncertainties in the angles represent the variation over the entire ensemble of structures determined by NMR.

in dark and light blue, respectively, in Figure 9). Closer inspection reveals that the interhelical angle of EF-3 changes noticeably from 118° (Ca^{2+} free) to 91° (Ca^{2+} bound) (see Table 1). The Ca^{2+}-induced decrease in the interhelical angle resembles somewhat the familiar Ca^{2+}-induced "closed" to "open" transition of EF-hands first observed for troponin C (*38*, *40*) and later for calmodulin (*39*, *41*, *42*) as described by the Herzberg−James model (*38*). The Ca^{2+}-induced opening of EF-3 causes the N-terminal E-helix of EF-3 to pull upward (Figure 9), resulting in a significant displacement of the connected domain linker and EF-2. In addition, the Ca^{2+}-induced opening of EF-3 appears to cause a steric clash of residues at the domain interface (see residues I88 and L108 in Figure 9) that further promotes the displacement and rearrangement of EF-2 and EF-3. The Ca^{2+}-induced structural changes depicted in Figure 9 illustrate how the local structural change within EF-3 results in the rearrangement of EF-2 and EF-3 at the domain interface that overall can be represented as a swiveling of the two domains.

In summary, the overall three-dimensional structure of Ca^{2+}-bound E85Q is unique and represents a hybrid of the structures of recoverin with zero and two Ca^{2+} bound. A distinctive feature of Ca^{2+}-bound myr-E85Q is that the carbonyl end of the fatty acyl group is more solvent exposed than it is in Ca^{2+}-free wild type (Figure 8). In contrast, the

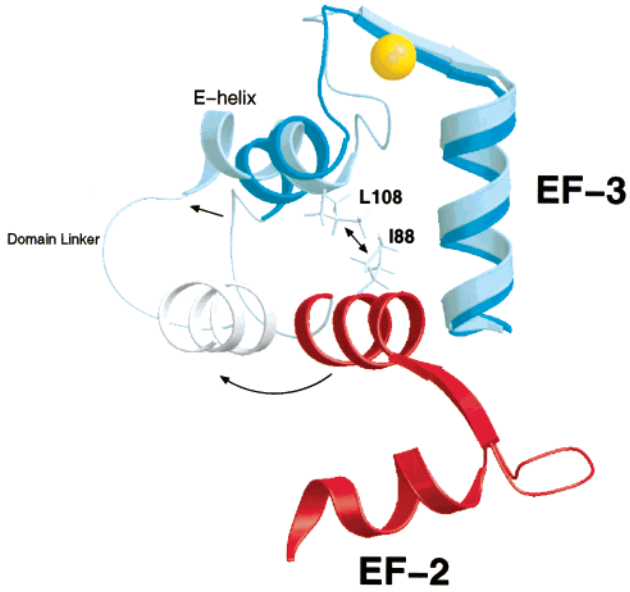

FIGURE 9: Ca^{2+}-induced structural changes within EF-3. Overlay of the main-chain structure of Ca^{2+}-free wild type (*13*) (EF-2, dark red, and EF-3, dark blue) compared with that of Ca^{2+}-bound myr-E85Q [C-terminal helix of EF-2 (residues 83−92), light red, and EF-3, light blue]. The structures of Ca^{2+}-free (dark blue) and Ca^{2+}-bound (light blue) EF-3 are superimposed (overall RMS deviation of main-chain atoms is 2.5 Å). The N-terminal E-helix and binding loop of EF-2 from the structure of Ca^{2+}-bound myr-E85Q are not shown for clarity. The side-chain atoms of I88 and L108 are indicated and illustrate possible Ca^{2+}-induced steric interactions that may help to promote the rearrangement of EF-2 and EF-3 at the domain interface.

C_{14}-methyl group of the myristate is buried inside the protein like that of Ca^{2+}-free wild type. The binding of Ca^{2+} to EF-3 causes structural changes within the EF-hand itself that sterically promotes a 45° swiveling of the two domains about the central linker. The swiveling of domains is functionally important because it displaces the C-terminal domain away

from the amino terminus (see residues W104 and L108 in Figure 7A,B), causing a partial unclamping of the myristoyl group.

DISCUSSION

In this study we present the structure and Ca^{2+}-binding properties of a myristoylated recoverin mutant (myr-E85Q) that binds Ca^{2+} to EF-3 (and not EF-2) and represents an intermediate state in the Ca^{2+}−myristoyl switch. Our equilibrium Ca^{2+}-binding studies of E85Q recoverin verify that Ca^{2+} binds only to EF-3 under all conditions used in this study (Figure 1). Our analysis of Ca^{2+} binding to unmyristoylated E85Q reveals that Ca^{2+} binds to EF-3 with nearly 100-fold higher intrinsic affinity than it does to EF-2. Consequently, we suggest that Ca^{2+} binds to EF-3 *first*, followed by subsequent and lower affinity binding to EF-2. The relatively low apparent affinity of Ca^{2+} binding to myr-E85Q (K_d = 100 μM) suggests that much of the binding energy is harnessed to drive a large conformational change in the myristoylated protein. Indeed, the structure of Ca^{2+}-bound myr-E85Q determined in this study reveals a substantial overall protein conformational change induced by the binding of Ca^{2+} to EF-3 (Figure 7A,B). Surprisingly, the local Ca^{2+}-induced structural changes within EF-3 appear rather modest. The RMS deviation of the main-chain atoms of EF-3 is only 2.5 Å in comparing Ca^{2+}-bound myr-E85Q with Ca^{2+}-free wild type. The Ca^{2+}-induced changes within EF-3 (Figure 9) resemble closely the Ca^{2+}-induced opening of EF-hands observed previously for calmodulin and troponin C (*38*) and contrast with the preformed closed structure of EF-hands found in calbindin D_{9k} (*43*−*45*). The interhelical angle of EF-3 decreases noticeably in the Ca^{2+}-bound state (see Table 1), which causes the E-helix to pull upward on the domain linker (Figure 9). As a consequence, the exiting helix of EF-2 (shaded pink in Figure 9) is displaced far away from EF-3 at the domain interface, resulting in a 45° swiveling of the two domains centered near Gly 96 (Figures 6B and 7B).

An important structural consequence of the domain swiveling is that it leads to a partial unclamping and exposure of the carbonyl end of the myristoyl group. The myristoyl group is highly sequestered in the Ca^{2+}-free protein because of its interaction with the C-terminal residues W104 and L108 (Figure 8A). The hydrophobic residues W104 and L108 are spatially close to the carbonyl end of the myristoyl group in the Ca^{2+}-free protein (Figure 8A) and are displaced far away from the fatty acid in the intermediate state (Figures 6B, 7B, and 8B).

The swiveling of the two domains also changes the packing interaction between EF-2 and EF-3 at the domain interface (compare H68 and L108 in Figure 7A,B) and may explain the observed positive cooperativity of Ca^{2+} binding to the myristoylated wild-type protein (*15*). The altered packing interaction between EF-2 and EF-3 in the intermediate state alters the structural environment of EF-2. As a consequence, the binding affinity of EF-2 would be expected to increase in the intermediate state and thereby promote the binding of a second Ca^{2+} to the protein at EF-2 (Figure 7B,C). The structure of unoccupied EF-2 in the intermediate state is somewhat different from that of Ca^{2+}-bound EF-2 (Figure 10). The interhelical angle of EF-2 decreases slightly

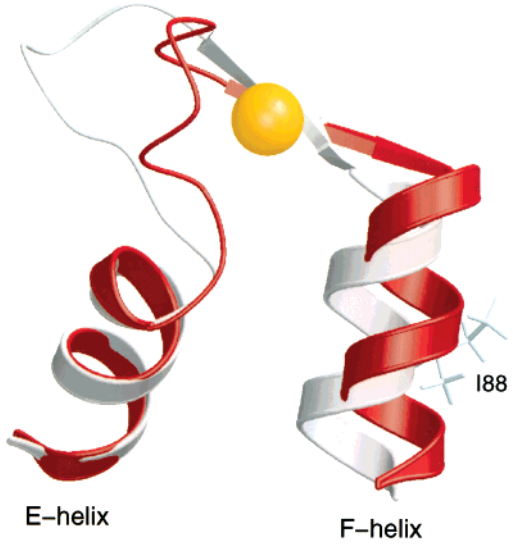

FIGURE 10: Ca^{2+}-induced structural changes within EF-2. Overlay of the main-chain structure of EF-2 from Ca^{2+}-free wild type (*13*) compared with that of Ca^{2+}-bound myr-E85Q. The structures of Ca^{2+}-free (dark red) and Ca^{2+}-bound (light red) EF-2 are superimposed (overall RMS deviation of main-chain atoms is 2.9 Å).

in the Ca^{2+}-bound state (Table 1), and the exiting F-helix rotates clockwise a few degrees about the central helical axis. Hence, these Ca^{2+}-induced structural changes of EF-2 are not energetically favorable in the closed T-state structure (Figure 7A) because the F-helix of EF-2 interacts sterically with Ca^{2+}-free EF-3 (see I88 and L108 in Figure 9). In contrast, the Ca^{2+}-induced displacement of the F-helix of EF-2 should become more favorable in the relatively open intermediate state (Figure 7B) because the F-helix of EF-2 in the intermediate state is not sterically restricted. Consistent with this interpretation, the E121Q mutant, in which EF-3 is inactivated, does not exhibit any Ca^{2+}-induced fluorescence change, suggesting that EF-2 is not permitted to undergo any Ca^{2+}-induced conformational change when EF-3 is unoccupied (*17*).

The binding of a second Ca^{2+} to the protein at EF-2 leads to structural changes within the N-terminal domain described previously (*14*) that directly lead to the ejection of the fatty acid (Figure 7B,C). The Ca^{2+}-induced structural changes of EF-2 (Figure 10) are propagated directly to EF-1 through interactions between the helices of EF-1 and EF-2. The helices of EF-1 are nearly antiparallel in the intermediate state (Figure 7B, when EF-2 is unoccupied) and become perpendicular upon binding of Ca^{2+} to EF-2 (Figure 7C). Swiveling at G42 in the loop between the helices of EF-1 (Figure 7C) moves the E-helix of EF-1 outward, causing it to pull on residues G2 to E26 on the N-terminal side of the helix. This N-terminal displacement allows the myristoyl group to swing out of its binding cavity. The ejection of the myristoyl group is further promoted by the partial unraveling of the N-terminal helix (K5 to E16) that causes residues G2 to A8 to become part of a flexible arm that places the myristoyl group outside and gives it freedom to insert into membrane targets.

The structure of Ca^{2+}-bound myr-E85Q presented here reveals that the amino-terminal myristoyl group is at least partially sequestered. Therefore, unlike the wild-type protein, the Ca^{2+}-bound myr-E85Q should not exhibit any appreciable

binding to membranes and might not inhibit rhodopsin kinase. Consistent with these predictions, recent work by Alekseev et al. (*22*) showed that the Ca^{2+}-bound myr-E85Q protein does *not* bind to membranes and does not inhibit rhodopsin kinase activity. Furthermore, the lack of any rhodopsin kinase inhibition by E85Q recoverin suggests that the extrusion of the myristoyl group (Figure 7C) might be essential for the interaction with the kinase. In contrast, a related mutant of frog S-modulin (E85M) did show some Ca^{2+}-induced binding to membranes (*19*). The reason for the discrepancy in the membrane-binding data of bovine E85Q and frog E85M mutants is currently unclear. A possible explanation might be that slight differences in the amino acid sequences of bovine recoverin and frog S-modulin (80% identical) could alter the energetics for the Ca^{2+}−myristoyl switch such that the binding of one Ca^{2+} would be sufficient to extrude the fatty acid in S-modulin but not in bovine recoverin.

Our structure of Ca^{2+}-bound myr-E85Q (that contains Ca^{2+} bound solely to EF-3) is different from the X-ray structure of unmyristoylated recoverin containing a single Ca^{2+} bound to EF-3 (*18*). The apparent differences in these structures can be explained by the allostery introduced by the attached myristoyl group (*15*). The allosteric effects of the myristoyl group have been described previously by a two-state concerted model (*15*), which also explains the dramatic differences in the Ca^{2+}-binding properties of myristoylated and unmyristoylated recoverin. In the allosteric model, two stable conformational states of the protein are postulated (T and R). The myristoyl group is sequestered in the T-state and extruded in the R-state. Therefore, the myristoyl group serves as an allosteric effector that stabilizes the T form. The myristoylated protein occupies the T-state in the absence of Ca^{2+} and switches to the R form upon binding two Ca^{2+}. In contrast, the unmyristoylated protein is always in the R-state regardless of the Ca^{2+} level because the T-state is unstable without the fatty acid. The lack of allostery ($L = 0$) for the unmyristoylated protein explains the similarity of the structures of unmyristoylated recoverin with one Ca^{2+} bound (*18*) and two Ca^{2+} bound (*46*). In contrast, the structure of myristoylated recoverin with one Ca^{2+} bound presented in this study is intermediate between the T and R forms. The structures of various intermediate species of hemoglobin were also observed recently to be trapped halfway between the T- and R-states (*47*, *48*).

In conclusion, the kinetic conversion of recoverin from T to R, which takes place during the Ca^{2+}−myristoyl switch, occurs via a two-step sequential mechanism as illustrated in Figure 7. To our knowledge, the structure of myristoylated recoverin containing one bound Ca^{2+} presented in this study is one of the most detailed structural characterizations of an intermediate species involved in an allosteric transition.

ACKNOWLEDGMENT

We thank the Keck Foundation for financial support and Frank Delaglio and Dan Garrett for writing computer software for NMR data processing and analysis.

REFERENCES

1. Polans, A., Baehr, W., and Palczewski, K. (1996) *Trends Neurosci. 19*, 547−554.
2. Palczewski, K., Polans, A. S., Baehr, W., and Ames, J. B. (2000) *BioEssays 22*, 337−350.
3. Yarfitz, S., and Hurley, J. B. (1994) *J. Biol. Chem. 269*, 14329−14332.
4. Dizhoor, A. M., Ray, S., Kumar, S. Niemi, G., Spencer, M., Rrolley, D., Walsh, K. A., Philipov, P. P., Hurley, J. B. and Stryer, L. (1991) *Science 251*, 915−918.
5. Gray-Keller, M. P., Polans, A. S., Palczewski, K., and Detwiler, P. B. (1993) *Neuron 10*, 523−531.
6. Erickson, M. A., Lagnado, L., Zozulya, S., Neubert, T. A., Stryer, L., and Baylor, D. A. (1998) *Proc. Natl. Acad. Sci. U.S.A. 95*, 6474−6479.
7. Kawamura, S. (1993) *Nature 362*, 855−857.
8. Polans, A. S., Buczylko, J., Crabb, J., and Palczewski, K. (1991) *J. Cell Biol. 112*, 981−989.
9. Maeda, T., Maeda, A., Maruyama, I., Ogawa, K., Kuroki, Y., Sahara, H., Sato, N., and Ohguro, H. (2001) *Invest. Ophthalmol. Visual Sci. 42*, 705−712.
10. Dizhoor, A. M., Ericsson, L. H., Johnson, R. S., Kumar, S., Olshevskaya, E., Zozulya, S., Neubert, T. A., Stryer, L., Hurley, J. B., and Walsh, K. A. (1992) *J. Biol. Chem. 267*, 16033−16036.
11. Zozulya, S., and Stryer, L. (1992) *Proc. Natl. Acad. Sci. U.S.A. 89*, 11569−11573.
12. Dizhoor, A. M., Chen, C. K., Olshevskaya, E., Sinelnikova, V. V., Phillipov, P., and Hurley, J. B. (1993) *Science 259*, 829−832.
13. Tanaka, T., Ames, J. B., Harvey, T. S., Stryer, L., and Ikura, M. (1995) *Nature 376*, 444−447.
14. Ames, J. B., Ishima, R., Tanaka, T., Gordon, J. I., Stryer, L., and Ikura, M. (1997) *Nature 389*, 198−202.
15. Ames, J. B., Porumb, T., Tanaka, T., Ikura, M., and Stryer, L. (1995) *J. Biol. Chem. 270*, 4526−4533.
16. Baldwin, A. N., and Ames, J. B. (1998) *Biochemistry 37*, 17408−17419.
17. Permyakov, S. E., Cherskaya, A. M., Senin, I. I., Zargarov, A. A., Alekseev, A. M., Zinchenko, D. V., Philippov, P. P., Uversky, V. N., and Permyakov, E. A. (2000) *Protein Eng. 13*, 783−790.
18. Flaherty, K. M., Zozulya, S., Stryer, L., and McKay, D. B. (1993) *Cell 75*, 709−716.
19. Matsuda, S., Hisatomi, O., Ishino, T., Kobayashi, Y., and Tokunaga, F. (1998) *J. Biol. Chem. 273*, 20223−20227.
20. Calvert, P. D., Klenchin, V. A., and Bownds, M. D. (1995) *J. Biol. Chem. 270*, 24127−24129.
21. Klenchin, V. A., Calvert, P. D., and Bownds, M. D. (1995) *J. Biol. Chem. 270*, 16147−16152.
22. Alekseev, A. M., Shulga-Morskoy, S. V., Zinchenko, D. V., Shulga-Morskaya, S. A., Suchkov, D. V., Vaganova, S. A., Senin, I. I., Zargarov, A. A., Lipkin, V. M., Akhtar, M., et al. (1998) *FEBS Lett. 440*, 116−118.
23. Kunkel, T. A. (1985) *Proc. Natl. Acad. Sci. U.S.A. 82*, 488−492.
24. Ray, S., Zozulya, S., Niemi, G. A., Flaherty, K. M., Brolley, D., Dizhoor, A. M., McKay, D. B., Hurley, J., and Stryer, L. (1992) *Proc. Natl. Acad. Sci. U.S.A. 89*, 5705−5709.
25. Ladant, D. (1995) *J. Biol. Chem 270*, 3179−3185.
26. Paulus, H. (1969) *Anal. Biochem. 32*, 91−100.
27. Ames, J. B., Hendricks, K. B., Strahl, T., Huttner, I. G., Hamasaki, N., and Thorner, J. (2000) *Biochemistry 39*, 12149−12161.
28. Ames, J. B., Tanaka, T., Ikura, M., and Stryer, L. (1995) *J. Biol. Chem. 270*, 30909−30913.
29. Tanaka, T., Ames, J. B., Kainosho, M., Stryer, L., and Ikura, M. (1998) *J. Biomol. NMR 11*, 135−152.
30. Brünger, A. T. (1992) *X-PLOR, Version 3.1: A System for X-ray Crystallography and NMR*, Yale University Press, New Haven, CT.
31. Badger, J., Kumar, R. A., Yip, P., and Szalma, S. (1999) *Proteins 35*, 25−33.
32. Bagby, S., Harvey, T. S., Eagle, S. G., Inouye, S., and Ikura, M. (1994) *Structure 2*, 107−122.
33. Bourne, Y., Dannenberg, J., Pollmann, V. V., Marchot, P., and Pongs, O. (2001) *J. Biol. Chem. 276*, 11949−11955.

34. Vijay-Kumar, S., and Kumar, V. D. (1999) *Nat. Struct. Biol. 6*, 80−88.
35. Freifelder, D. (1982) in *Physical Biochemistry: Applications to Biochemistry and Molecular Biology*, pp 537−572, W. H. Freeman and Co., San Francisco, CA.
36. Ames, J. B., Tanaka, T., Stryer, L., and Ikura, M. (1994) *Biochemistry 33*, 10743−10753.
37. Babu, Y. S., Bugg, C. E., and Cook, W. J. (1988) *J. Mol. Biol. 204*, 191−204.
38. Herzberg, O., and James, M. N. (1988) *J. Mol. Biol. 203*, 761−779.
39. Zhang, M., Tanaka, T., and Ikura, M. (1995) *Nat. Struct. Biol. 2*, 758−767.
40. Gagne, S. M., Tsuda, S., Li, M. X., Smillie, L. B., and Sykes, B. D. (1995) *Nat. Struct. Biol. 2*, 784−789.
41. Kuboniwa, H., Tjandra, N., Grzesiek, S., Ren, H., Klee, C. B., and Bax, A. (1995) *Nat. Struct. Biol. 2*, 768−776.
42. Finn, B. E., Evenas, J., Drakenberg, T., Waltho, J. P., Thulin, E., and Forsen, S. (1995) *Nat. Struct. Biol. 2*, 777−783.
43. Maler, L., Blankenship, J., Rance, M., and Chazin, W. J. (2000) *Nat. Struct. Biol. 7*, 245−250.
44. Skelton, N. J., Kordel, J., Akke, M., Forsen, S., and Chazin, W. J. (1994) *Nat. Struct. Biol. 1*, 239−245.
45. Nelson, M. R., Thulin, E., Fagan, P. A., Forsen, S., and Chazin, W. J. (2002) *Protein Sci. 11*, 198−205.
46. Ames, J. B., Tanaka, T., Stryer, L., and Ikura, M. (1996) *Curr. Opin. Struct. Biol. 6*, 432−8.
47. Fernandez, E. J., Abad-Zapatero, C., and Olsen, K. W. (2000) *J. Mol. Biol. 296*, 1245−1256.
48. Schumacher, M. A., Zheleznova, E. E., Poundstone, K. S., Kluger, R., Jones, R. T., and Brennan, R. G. (1997) *Proc. Natl. Acad. Sci. U.S.A. 94*, 7841−7844.

BI012153K